

UC San Diego

UC San Diego Previously Published Works

Title

Analysis of the cloud enhancement phenomenon and its effects on photovoltaic generators based on cloud speed sensor measurements

Permalink

<https://escholarship.org/uc/item/2x93f1fs>

Journal

Journal of Renewable and Sustainable Energy, 12(4)

ISSN

1941-7012

Authors

Lappalainen, Kari
Kleissl, Jan

Publication Date

2020-07-01

DOI

10.1063/5.0007550

Peer reviewed

1 Analysis of the cloud enhancement phenomenon and its effects on photovoltaic 2 generators based on cloud speed sensor measurements

3 4 Authors:

5 Kari Lappalainen¹, kari.lappalainen@tuni.fi

6 Jan Kleissl², jkleissl@ucsd.edu

7 ¹Tampere University, Electrical Engineering Unit, P.O. Box 692, FI-33101 Tampere, Finland

8 ²University of California, San Diego, Department of Mechanical and Aerospace Engineering, CA
9 92093-0411, United States

10 11 Abstract

12
13 The irradiance incident on photovoltaic (PV) generators can considerably exceed the expected
14 clear sky irradiance. Due to this phenomenon, called cloud enhancement (CE), the maximum power
15 of the PV generator can exceed the rated power of the inverter connecting the generator to grid. CE
16 event characteristics and the effects of CE on the electrical operation of PV generators were studied
17 based on measured irradiances and cloud edge velocities. Over eleven months in San Diego,
18 California, the highest measured peak irradiance was 1466 W/m². In addition, the highest simulated
19 average irradiances for up to 1 MW generators were over 1400 W/m². The largest lengths for CE
20 events exceeding 1000 W/m² were multiple kilometers. These results indicate that even large utility-
21 scale PV power plants can be affected significantly by CE events. Moreover, the operation of three
22 PV plants was simulated during around 2400 measured CE events with a detailed spatio-temporal
23 model down to a PV submodule. The effects of inverter sizing on the operation of the plants were
24 also studied and the negative impacts of CE on the operation of PV systems were shown to increase
25 with increasing DC/AC ratio. The operating voltage increased with increasing DC/AC ratio and
26 decreasing plant size and the highest operating voltages were 25% higher than nominal. During the
27 CE events, the energy losses due to power curtailment were from 5% to 50% of the available energy
28 production increasing with increasing DC/AC ratio. While CE affects the operation of the PV plants,
29 these effects were small in terms of aggregate energy, since CE events that most strongly impact PV
30 system operation are very rare, meaning that CE do not cause major problems for the operation of PV
31 systems.

32 33 1. Introduction

34
35 The operation of photovoltaic (PV) generators depends on the irradiance incident on the PV
36 cells of the generator. While solar radiation is variable (Tomson, 2013; Lappalainen and Valkealahti,
37 2015), the nominal electrical characteristics of PV modules are typically defined under the standard
38 test conditions (STC), i.e., at an irradiance of 1000 W/m² and a cell temperature of 25 °C. However,
39 these conditions are rare in practice. In many parts of the world, clear sky irradiance, i.e., the global
40 irradiance from cloudless sky, can be higher than the STC irradiance around solar noon (Badescu,
41 1997). Moreover, on partly cloudy days, irradiance can considerably exceed the expected clear sky

42 irradiance due to a phenomenon called cloud enhancement (CE), irradiance enhancement (Pecenak
43 et al., 2016) or overirradiance (Yordanov et al., 2013a).

44 Irradiance levels exceeding 1000 W/m² (depending on module temperature) can cause the
45 actual power of the generator to exceed its nominal maximum power. Zehner et al. (2011) reported
46 up to 30% higher power output of PV modules under high irradiance conditions compared to the STC.
47 High irradiance conditions can lead to the maximum PV power exceeding the maximum DC power
48 of the inverter connecting the PV generator to grid. Moreover, PV capacity is typically oversized such
49 that the nominal DC power of the PV generator is higher than the inverter nominal (AC) power (Wang
50 et al., 2018). If the maximum power of the PV generator is higher than the maximum DC power of
51 the inverter, the inverter will operate in power limiting mode: By moving the inverter operating point
52 to higher voltages than those at the global maximum power point (MPP) of the generator, the current
53 and power of the inverter decrease.

54 In addition to the loss of available energy production, operating in power limiting mode
55 negatively effects the operation and efficiency of the inverter: (i) The efficiency of some inverters
56 decreases with increasing DC side voltage (Rampinelli et al., 2014) causing further losses in AC
57 power output. (ii) The inverter capacitor lifetime shortens with increasing DC voltage (Hasegawa et
58 al., 2018; Callegari et al., 2019). (iii) Under extreme conditions the voltage required to reduce output
59 power may be outside the allowed voltage range of the inverter.

60 Under clear sky conditions, irradiances exceeding 1000 W/m² are typically not an issue as the
61 exceedance is less than 10% in most areas of the world (except for high altitudes) and PV efficiency
62 losses due to high panel temperature typically far exceed 10% compared to PV efficiency at 25 °C.
63 However, during CE irradiance can be much larger and PV temperatures are typically lower.
64 Gueymard (2017a) postulated that there are three types of CE effects that can strongly increase global
65 horizontal irradiance (GHI): 1) the traditional explanation of CE phenomenon: the enhancement of
66 irradiance due to cloud edges near the solar disk; 2) increase of diffuse horizontal irradiance under a
67 homogenous cloud deck before and after a CE event; and 3) partial obscuration of the sun by a thin
68 cloud layer, while most of the sky is covered by bright clouds. In type 3, the share of diffuse irradiance
69 is large while the amount of direct horizontal irradiance is much lower than in types 1 and 2. Yordanov
70 et al. (2013a) demonstrated that the strongest CE is due to strong forward scattering within a small
71 angle around the solar disk. That kind of a situation may occur when the sun appears in a narrow gap
72 between clouds within 5° around the solar disk, which are thin enough to strongly forward scatter.
73 Increases over 1000 W/m² can be substantial: Gueymard (2017b) measured global tilted irradiance
74 (GTI) of almost 2.0 kW/m² for a 40° tilt angle and GHI of almost 1.9 kW/m² in Colorado at 1829 m
75 elevation, Nascimento et al. (2019) reported GHI of over 1.8 kW/m² at elevations of 392 m and 32 m
76 in Brazil and Yordanov et al. (2015) measured GTI of 1.6 kW/m² near sea level at a latitude close to
77 60°N.

78 Although CE is well-known phenomenon, its characteristics relevant to the operation of PV
79 systems, such as duration and spatial extent, have not received much attention. The durations of CE
80 events were studied in some articles: Yordanov et al. (2013a) presented duration distributions for CE
81 events exceeding 1100 W/m²; Zhang et al. (2018) studied the duration of CE events exceeding clear
82 sky irradiance; and Järvelä et al. (2020) studied the duration of CE events with various irradiance
83 limits over the land area of various PV generators. Järvelä et al. (2018, 2020) studied the land area

84 lengths of CE events in Finland based on irradiance measurements and by invoking Taylor's
85 hypothesis. They found typical CE event lengths to be on the order of hundreds of meters. Espinosa-
86 Gavira et al. (2018) showed that CE can extend over land areas of 15×15 m. Weigl et al. (2012)
87 showed that the land areas of CE events can be large enough to affect the operation of utility-scale
88 PV power plants.

89 The effects of CE on the operation of PV systems have been studied in few articles: Zehner
90 et al. (2011) studied the operation of individual PV modules under CE; Luoma et al. (2012) studied
91 inverter sizing and energy losses due to inverter saturation under CE; Weigl et al. (2012) studied the
92 operation of PV systems under a single CE situation; and Nascimento et al. (2019) studied the effects
93 of CE events on the performance of PV generators focusing mainly on combiner box fuses. Tapakis
94 and Charalambides (2014) discussed the possible effects of CE on PV inverters.

95 This article presents a study of CE event characteristics and the effects of CE on the electrical
96 operation of PV generators. The study is based on measurements of GHI and cloud edge velocity
97 from San Diego, California. First, the number, duration, and land area length of CE events exceeding
98 various irradiance limits over the land areas of various PV generators are studied. After that, the
99 operation of three PV plants, ranging from 20 to 200 kW, is simulated during around 2400 measured
100 CE events exceeding 1000 W/m². Moreover, the effects of inverter sizing on the operation of the PV
101 plants are studied. The main novelty of this study is that, for the first time, the detailed (down to the
102 submodule) electrical operation of PV generators is extensively studied under CE based on actual
103 irradiance measurements.

104 The rest of this article is organized as follows. Sections 2.1–2.4 introduce the measurement
105 data and the methods used to study the characteristics of CE events in terms of irradiance. The results
106 of these studies are presented in Sections 2.5–2.7. The methods used to study the effects of CE on the
107 operation of PV generators are presented in Sections 3.1 and 3.2. Section 3.3 illustrates the effects of
108 CE on the operation of PV generators by two static example CE situations. The statistics during all
109 the CE events identified in measured irradiance are presented in Section 3.4. The results are further
110 discussed in Section 4 and the conclusions are given in Section 5.

111

112 **2. Cloud enhancement events**

113

114 In this section, characteristics of CE events are studied in terms of irradiance magnitudes,
115 enhancement durations, and for point irradiance as well as the estimated average irradiances of
116 various PV generator land areas. This section investigates how often and how long typical land areas
117 of different PV generator sizes experience CE.

118

119 **2.1. Measurement data**

120

121 The study is based on measurement data of a GHI sensor (LI-200, LI-COR Inc., USA) and a
122 cloud speed sensor (CSS) installed on the rooftop of the EBU2 building at the University of
123 California, San Diego (UCSD) ($32^{\circ}52'53''\text{N}$, $117^{\circ}13'59''\text{W}$). The GHI measurements were performed
124 with a sampling frequency of 0.5 Hz while the response time of the sensor is 10 μs . The CSS,
125 presented in Fig. 1, consists of an array of nine phototransistors (TEPT4400, Vishay Intertechnology

126 Inc., USA) (Wang et al., 2016). The phototransistors form a circular sector with a radius of 29.7 cm
127 and a central angle of 105° . Eight of the phototransistors are located at the arc of the circular sector
128 around the ninth phototransistor that is positioned at the center of the circle. The data acquisition rate
129 of the CSS is irregular since it requires cloud edge passages to determine cloud motion vectors
130 (CMVs). The minimum time between produced CMVs is 11 s, which is sufficient for cloud motion
131 estimation in the scope of this study. The procedure to calculate CMVs is presented in the Appendix.
132 The shadow movement direction is defined as direction where clouds come from relative to north.
133 CMVs were determined during 62 days from October 2017 to August 2018 from which also GHI
134 measurements were available. All these days, which compose the used dataset, were partially cloudy.
135



136
137 Fig. 1. Cloud speed sensor contained in an enclosure.
138

139 2.2. Identification of cloud enhancement events

140

141 A CE event is often defined by comparing measured irradiance to expected clear sky
142 irradiance (Yordanov et al., 2015; Zhang et al., 2018). In that way, a CE event starts when the
143 irradiance exceeds the clear sky irradiance and ends when the irradiance decreases below the clear
144 sky irradiance. However, from PV system operation point of view, a more sensible way is to use a
145 static irradiance value as a reference instead of the clear-sky irradiance that is location-specific. On
146 the other hand, the use of a static irradiance value as the limit of CE events has the drawback that,
147 depending on the location, non-CE events with large clear sky irradiance may be included, or
148 situations with real CE during small clear sky irradiance that do not reach the static threshold may be
149 excluded from the study. A typical static value used to define CE events is the solar constant (Zhang
150 et al., 2018). However, the use of solar constant is not justified from the PV power operation point of
151 view. Since the nominal ratings of PV modules are typically defined under STC, from PV system
152 operation point of view, a more reasonable choice for a static threshold is the STC irradiance of
153 1000 W/m^2 . To make the results more generalizable, instead of using a single static irradiance limit,
154 we opted to use a continuous range of irradiance values starting from 1000 W/m^2 and identified all
155 events where the measured irradiance, or estimated average irradiance, exceeded the irradiance limit.
156 Then, we systematically counted the numbers and durations of these events for each irradiance limit.
157

158 2.3. PV generator land areas

159

160 Average irradiances over the land areas of various PV generators were estimated. The nominal
 161 powers, side lengths, and land areas of the studied virtual PV generators are compiled in Table I. The
 162 land areas are based on typical land areas of PV generators with these power ratings (Ong et al.,
 163 2013). The selected power ratings correspond to typical power ratings of medium-sized (0.05 MW)
 164 and large (0.2 MW) string inverters, and medium-sized (1 MW) and large (4 MW) central inverters.
 165 The PV generators were assumed to have a square shape. The shape of PV generators varies greatly
 166 in practice. The shape of the generator affects the cumulative time the PV generators experience CE.
 167 The use of a square shape is justified as it is the most typical in practice. An oblong generator shape
 168 could distort the results more than a square shape: if one dimension of the generator is very short
 169 compared to the other, a small CE area (from a near-perpendicular direction) could fully cover the
 170 generator while it could not cover a square shaped generator of the same area.

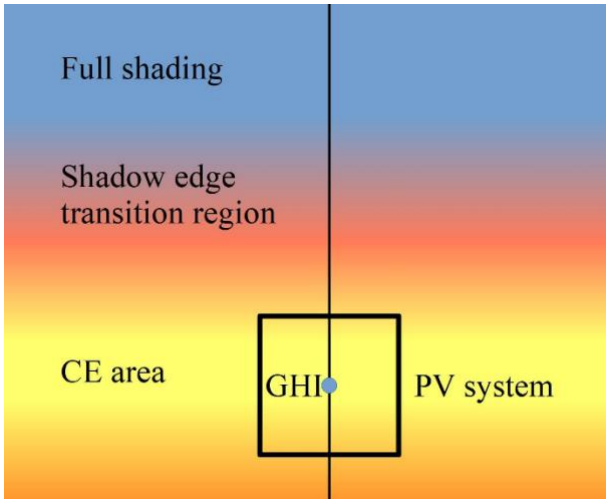
171
 172 Table I. The powers, side lengths, and land areas of the studied PV generators.

Nominal power (MWp)	Side length	Area (m ²)
0.05	25	625
0.20	50	2500
1.00	125	15625
4.00	250	62500

173
 174 2.4. Assumptions and estimation of 2D average irradiances
 175

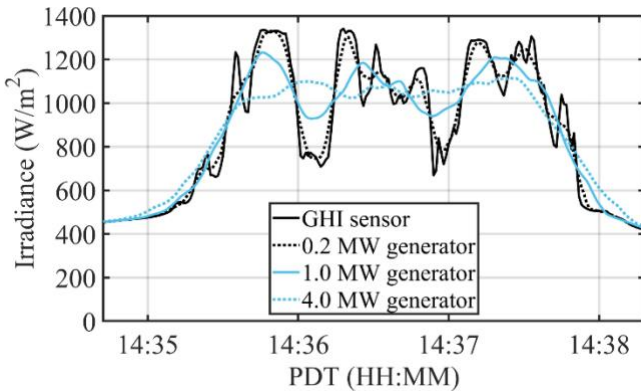
176 Since CE events are the result of light scattering by clouds, the speeds and movement
 177 directions of the CE areas can be estimated based on the measured CMVs. The average irradiance of
 178 the PV generator was estimated from measured point irradiance based on three assumptions: 1)
 179 Taylor’s hypothesis in the streamwise direction; 2) uniformity in the cross-stream direction; and 3)
 180 the CE areas move perpendicular to the PV generator side. Through these assumptions, the CE areas
 181 can be studied one-dimensionally allowing straightforward calculation of the average irradiances over
 182 the PV generator land areas. The assumptions and the movement of a CE area are illustrated in Fig. 2.

183 The assumptions are reasonable for the studied PV generator sizes. However, assumption 2
 184 becomes less reasonable and the uncertainty of the results therefore increases with increasing land-
 185 area. Typical land area lengths of CE events have been found to be in the order of hundreds of meters
 186 up to several kilometers (Järvelä et al., 2018). Typical land area diameters of cloud shadows have
 187 been reported to be around 800 m (Lappalainen and Valkealahti, 2016). The resulting CE geometries
 188 differ from those occurring in reality since cloud and scattering geometries are three-dimensional and
 189 complex. However, dense measurement networks that cover the spatio-temporal evolution of CE are
 190 not available. The extrapolation from a timeseries at a point to a line in the wind direction (1D) is
 191 well documented and reasonable based on Taylor’s hypothesis, and given that the spatial scale of
 192 clouds is larger than the array sizes, the extrapolation from 1D to 2D also appears to be a reasonable
 193 assumption for the purposes of this study, which is to derive typical statistics for the effects of CE
 194 events on PV generators.



196
 197 Fig. 2. Conceptual bird's eye view of a CE event that is upwind of a cloud as it impacts a PV system. Irradiance
 198 increases from blue to red to yellow. The irradiance map is generated from time series at the GHI sensor (blue dot) that
 199 is converted to a line in space aligned with the direction of cloud motion using Taylor's hypothesis (black line,
 200 assumption 1) and extrapolated in the crosswind direction (assumption 2). The PV system borders are assumed to be
 201 perpendicular to the direction of motion (assumption 3).
 202

203 The average irradiance over the land area of the PV generator was calculated by averaging
 204 the measured irradiance over a time interval defined by the ratio of the PV generator dimension and
 205 the measured cloud shadow speed. Fig. 3 presents an example of the measured irradiance and the
 206 average irradiances over PV generators of different sizes. The irradiance profile becomes smoother
 207 for larger generator land areas. The peak irradiance decreases with increasing generator area, all PV
 208 generators experience average irradiances exceeding 1100 W/m².
 209



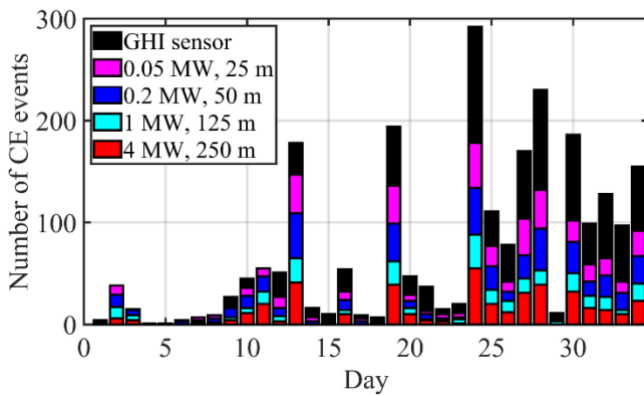
210
 211 Fig. 3. Irradiance measured with the GHI sensor and the corresponding average irradiances over land areas of 0.2, 1.0,
 212 and 4 MW PV generators on May 17, 2018.
 213

214 2.5. Number of cloud enhancement events

215
 216 The example in Fig. 3 illustrates the effect of generator land area on the number and duration
 217 of CE events identified in the estimated average irradiances of the generators. The irradiance
 218 measured by the GHI sensor exceeded 1000 W/m² eight times, i.e., the number of identified CE
 219 events for the limit of 1000 W/m² was eight. The estimated average irradiances of the 0.2 and 1 MW
 220 generators exceeded the limit of 1000 W/m² three times. For the 4 MW generator, only one CE event

221 was identified. However, the duration of this event was about two minutes, while the smaller
 222 generators and the point measurement experienced multiple shorter CE events. The number of CE
 223 events exceeding 1200 W/m² was eight, four and two for the point measurement, 0.2 MW and 1 MW
 224 generator, respectively. The largest average irradiance of the 4 MW generator was 1114 W/m². Thus,
 225 it did not experience a CE event exceeding 1200 W/m².

226 Irradiance values larger than the STC irradiance were measured during 34 days out of 62.
 227 Fig. 4 presents the daily numbers of identified CE events exceeding 1000 W/m². For clarity, only the
 228 days when CE was measured were included in this figure. On average, 39 CE events per day were
 229 identified in measured point irradiance. The average daily numbers of identified CE events were 24,
 230 18, 11, and 7 for the 0.05, 0.2, 1, and 4 MW generators, respectively. Considering only the days with
 231 measured CE events, on average 71 CE events per day occurred in the measured irradiance. The
 232 number of identified CE events decreased with increasing generator size due to the smoothing of
 233 irradiance with increasing land area. The largest number of CE events was identified on May 17,
 234 2018, with nearly 300 CE events in measured point irradiance and 55 CE events in the average
 235 irradiance of the 4 MW PV generator.
 236



237 Fig. 4. Daily numbers of CE events exceeding 1000 W/m² for the GHI sensor and the studied PV generators. The statistics
 238 in this figure are not representative for the occurrence of CE events since only the days when CE occurred were included
 239 in the analyses.
 240

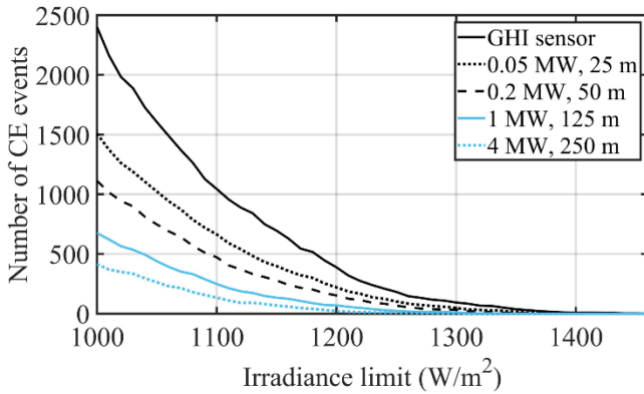
241
 242 The highest irradiances measured by the GHI sensor and the highest average irradiances for
 243 the studied PV generators are compiled in Table II. The highest measured irradiance was 1466 W/m².
 244 The highest average irradiances for the 0.05, 0.2, and 1 MW generators were over 1400 W/m², i.e.,
 245 over 1.4 times the STC irradiance. The highest average irradiance for the 4 MW generator was 1.34
 246 times the STC irradiance.
 247

248 Table II. Highest average irradiances for the GHI sensor and the studied PV generators over 62 days.

Area	Irradiance (W/m ²)
GHI sensor	1466
0.05 MW generator	1441
0.2 MW generator	1433
1 MW generator	1408
4 MW generator	1339

249

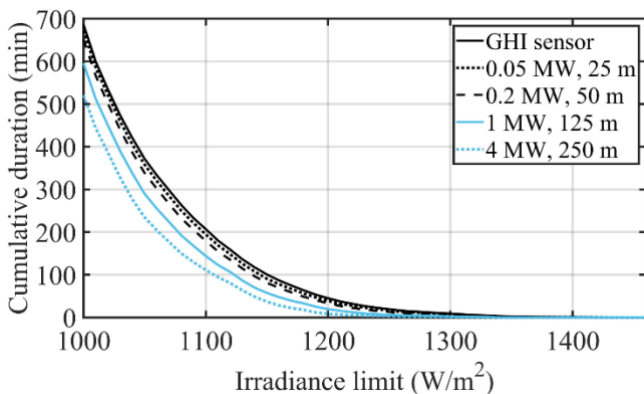
250 The numbers of identified CE events for the studied PV generators are presented in Fig. 5 as
 251 a function of irradiance limit. The number of the CE events decreased with increasing PV generator
 252 land area and with increasing average irradiance. The measured point irradiance exceeded the STC
 253 irradiance around 2400 times during the 62 days included in the analyses. The average irradiance of
 254 the 0.05 and 4 MW generator exceeded the STC irradiance over 1500 and 400 times, respectively.
 255



256
 257 Fig. 5. Numbers of the identified CE events as a function of irradiance limit.
 258

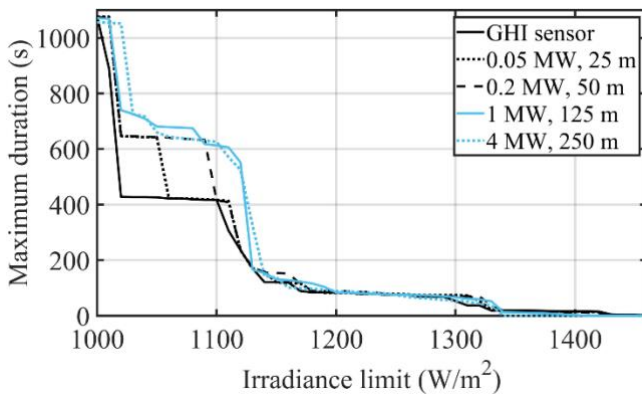
259 2.6. Duration of cloud enhancement events

260
 261 The cumulative durations of identified CE events for the PV generators are presented in Fig. 6
 262 as a function of irradiance limit. Naturally, the cumulative duration of the CE events decreased with
 263 increasing irradiance limit and increasing land area. The cumulative duration of the CE events
 264 exceeding 1000 W/m² was 11 hours and 27 minutes for the GHI sensor and 8 hours and 41 minutes
 265 for the 4 MW PV generator. The largest cumulative duration of CE events measured by the GHI
 266 sensor in one day was 1 hour and 40 minutes while the average daily duration was just over
 267 11 minutes indicating that energy losses due to operation in power limiting mode during CE events
 268 are not a major issue for PV generators. The cumulative irradiance part above the STC irradiance was
 269 12.3 kWh/m² for the GHI sensor and 9.2 kWh/m² for the 4 MW generator decreasing with increasing
 270 land area. For reference, a typical PV generator in San Diego produces about 1,500 kWh/m²/year or
 271 255 kWh/m² during the 62 days of the experiment.
 272



273
 274 Fig. 6. Cumulative durations of the identified CE events as a function of irradiance limit.
 275

276 Fig. 7 presents the maximum durations of CE events for the PV generators as a function of
 277 irradiance limit. The maximum durations decrease with increasing irradiance limit. The maximum
 278 durations of CE events exceeding 1000 W/m² were around 18 minutes. The average duration of these
 279 CE events was 17.2 s for the GHI sensor and increased with increasing land area up to 75.6 s for the
 280 4 MW PV generator. The reason for this is that small temporary dips in measured irradiance below
 281 1000 W/m² are smoothed out with larger land area and thus the average irradiance remains longer
 282 above 1000 W/m² as illustrated in Fig. 3. The longest durations of the strongest CE events with
 283 average irradiance exceeding 1400 W/m² were over ten seconds for the GHI sensor and the 0.05 and
 284 0.2 MW PV generators.
 285



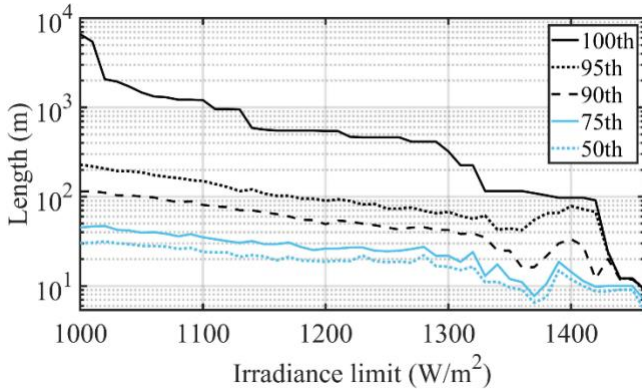
286
 287 Fig. 7. Maximum durations of the identified CE events as a function of irradiance limit.
 288

289 The measured durations of CE events are broadly consistent and slightly longer than those
 290 reported in Yordanov et al. (2013a) and Järvelä et al. (2020). For example, the maximum durations
 291 of CE events exceeding 1100 W/m² reported in Yordanov et al. (2013a) and Järvelä et al. (2020) were
 292 around 390 and 230 s, respectively, while in this study a duration of 420 s was measured. The
 293 differences result mainly from the geographical location. In Yordanov et al. (2013a), measurements
 294 were performed in Southern Norway (latitude 58°20'N) and the sensor was oriented south (173° from
 295 North) with a tilt angle of 39° (Imenes et al., 2011). In Järvelä et al. (2020), measurements were
 296 performed in Finland (latitude 61°75'N) with sensors oriented 23° east of due south with a tilt angle
 297 of 45°. In this study, the latitude was 32°53'N resulting in higher clear-sky maximum irradiance
 298 values because of smaller air mass even though GHI was measured, i.e. the sensor was not tilted.
 299 However, the measured CE event durations between these studies are broadly consistent given all the
 300 differences in the measurements.
 301

302 2.7. Length of cloud enhancement areas

303
 304 The land area length of each identified CE event was calculated by multiplying the measured
 305 duration of the event by the measured cloud shadow speed. CE area length quantiles are presented in
 306 Fig. 8 as a function of irradiance limit. The lengths of CE areas decreased with increasing irradiance
 307 limit. The largest lengths for CE events exceeding 1000 and 1100 W/m² were around 6.6 and 1.2 km,
 308 respectively, meaning that even large utility-scale PV power plants can be affected by CE events. A
 309 square-shaped 16 MW PV generator with a side length of 500 m can occasionally be totally covered

310 by a CE area with minimum irradiance of over 1200 W/m². A 4 MW generator (side length 250 m)
 311 can be fully covered by a CE area with minimum irradiance of over 1300 W/m². 25% and 50% of CE
 312 events exceeding 1250 and 1100 W/m², respectively, are large enough to fully cover a 0.05 MW PV
 313 generator. It is worth noting that the land area lengths were calculated along the CE area (cloud edge)
 314 movement direction. Naturally, full cover of PV generators requires that also the transverse size of a
 315 CE event is large enough.



317 Fig. 8. 100th, 95th, 90th, 75th, and 50th percentiles of CE area length as a function of irradiance limit.
 318

320 3. Effects of cloud enhancement on photovoltaic generators

321
 322 In this section, the effects of cloud enhancement on PV generators are studied by simulations.
 323 The electrical operation of three PV generators was simulated during all the identified CE events
 324 exceeding 1000 W/m² described in Section 2. This section investigates how CE affects the global
 325 MPP voltage and power of the PV generators, the fraction of time the generators spend in power
 326 limiting mode, and energy losses caused by power curtailment. Moreover, the effects of inverter
 327 sizing on the operation of the PV plants were studied by varying the DC/AC ratio, i.e., the ratio of
 328 the nominal PV DC power to the nominal inverter power.

330 3.1. Simulation model for the PV modules

331
 332 A PV submodule, i.e., a group of series-connected PV cells in a PV module protected by a
 333 bypass diode, was used as a basic unit in the simulations. The PV submodules were modeled by a
 334 MATLAB Simulink model, which utilizes the common one-diode model of a PV cell providing the
 335 following relationship between the current I and voltage U of a PV submodule:

$$336 \quad I = I_{ph} - I_o \left(e^{\frac{U + R_s I}{A k N_s T / q}} - 1 \right) - \frac{U + R_s I}{R_{sh}}, \quad (1)$$

337 where I_{ph} is the light-generated current, I_o the dark saturation current, A the ideality factor, T the
 338 operating temperature, R_s the series resistance, and R_{sh} the shunt resistance of the PV submodule. The
 339 Boltzmann constant is represented by k , N_s is the number of PV cells in the submodule and q is the
 340 elementary charge. The effect of irradiance G was taken into account when calculating I_{ph} as

341
$$I_{ph} = (I_{SC, STC} + K_I \Delta T) \frac{G}{G_{STC}} \frac{R_s + R_{sh}}{R_{sh}}, \quad (2)$$

342 where $I_{SC, STC}$ is the short-circuit (SC) current in STC, K_I the temperature coefficients of I_{SC} , and ΔT
 343 the temperature difference compared to STC. The bypass diodes were assumed to be at the same
 344 temperature as the submodules and were modeled using Eq. (1) by assuming I_{ph} to be zero and R_{sh}
 345 infinite. The characteristics of the simulation model were fitted to the characteristics of NAPS
 346 NP190GKg PV modules, which are composed of three submodules of 18 multicrystalline silicon PV
 347 cells. Details of the fitting process and the experimental verification of the simulation model are
 348 available in Mäki et al. (2012). Table III presents the SC current and open-circuit (OC) voltage of the
 349 submodule in STC and the parameter values of the simulation model.

350
 351 Table III. Parameter values of the simulation model for the PV submodules and bypass diodes.

Parameter	Value
$I_{SC, STC}$	8.02 A
$U_{OC, STC}$	11.0 V
A	1.30
K_I	4.70 mA/K
N_s	18
R_s	0.110 Ω
R_{sh}	62.6 Ω
A_{bypass}	1.50
$I_o, bypass$	3.20 μA
$R_s, bypass$	20.0 m Ω

352
 353 3.2. Modeling of PV generators under cloud enhancement events
 354

355 The electrical operation of three PV generators was studied during the CE events exceeding
 356 1000 W/m² described in Section 2. The STC irradiance of 1000 W/m² was selected as the limit since
 357 the nominal ratings of PV modules and PV generators are typically defined for this irradiance. The
 358 generators consisted of 6 parallel strings of 16 series-connected PV modules, 24 strings of
 359 20 modules, and 36 strings of 28 modules. These generator sizes correspond to typical ratings of
 360 small (6 × 16), medium-sized (24 × 20), and large (36 × 28) string inverters. The PV modules were
 361 installed facing south with a 20° tilt angle with respect to the horizon. The module strings were located
 362 in straight lines without gaps between the modules and with a 1.5 m gap between the strings. The
 363 details of the studied PV generators are compiled in Table IV.

364
 365 Table IV. Numbers of modules, powers, and dimensions of the studied PV generators.

Number of modules (parallel × series)	Nominal power (kWp)	Dimensions (m)	Area (m ²)
6 × 16	18.2	13.1 × 23.6	308
24 × 20	91.2	56.7 × 29.5	1674
36 × 28	191.5	85.9 × 41.3	3546

366
 367 The operation of the PV generators was studied during the movement of the identified CE
 368 events over the generators using assumptions 1) and 2) used earlier to estimate the average irradiances
 369 (see Section 2.4) with the difference that the CE areas were not assumed to move perpendicular to

370 the PV generator side but measured movement directions were used. Moreover, the CE area speed
371 and movement direction were assumed constant while the CE areas move over the PV generators.
372 The speeds and movement directions for the CE events were calculated from the measured CMVs.
373 The CMVs measured during a CE event were decomposed into north-south and east-west directions
374 and the median value of each was used to recombine one median filtered CMV, which was used for
375 the CE event.

376 A simulation period was the period when the CE area covered at least one submodule of the
377 PV generator, i.e., the simulation period started when the irradiance of the first PV submodule of the
378 generator exceeded the limit of 1000 W/m² and ended when the edge of the CE area moved away
379 from the last submodule. For each time step of 0.1 s, the irradiance at the center of a submodule was
380 taken as the irradiance of the submodule. The operating temperature of the PV submodules was 25 °C
381 during the simulations. Since temperature measurements over the land areas of the simulated
382 generators were not available and modeling temperature under transient conditions is a challenge, we
383 opted for this assumption. Note that Weigl et al. (2012) also assumed a constant PV module
384 temperature, albeit at 40 °C. The effects of this assumption are further discussed in Section 4. The
385 total duration of the identified CE events for the PV generators increased with increasing generator
386 land area, being around 135 hours for the smallest and 208 hours for the largest generator.

387 MPP tracking of the PV plants was assumed ideal, meaning that the generator is operating at
388 the global MPP unless it is in power limiting mode, i.e., the power at global MPP is higher than the
389 nominal power of the inverter. In that case, the generator is operating on the right-hand side of the
390 global MPP at the lowest voltage where the nominal power of the inverter is not exceeded. The
391 DC/AC ratio was varied from 1.0 to 2.0.

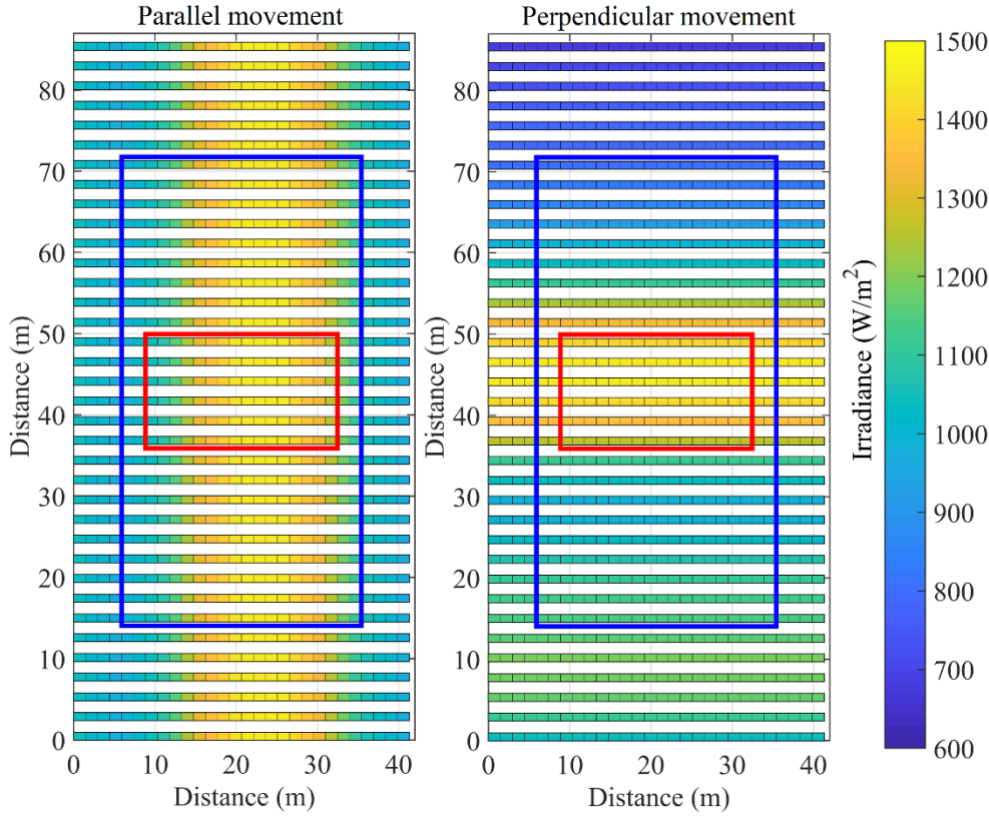
392

393 3.3. Static example cloud enhancement situations

394

395 The effects of CE on the operation of PV plants is first illustrated by two examples. In these
396 examples, the CE event with the largest measured irradiance (1466 W/m²) is located at the center of
397 the plants. Parallel and perpendicular CE area movement with respect to the strings of the plants are
398 considered. The irradiance levels received by the PV submodules of the plants are presented in Fig. 9
399 and average irradiances are compiled in Table V. The average irradiances decreased with increasing
400 plant size. The average irradiances of the 24 × 20 and 36 × 28 plants are larger in the case of parallel
401 CE area movement. However, the average irradiance of the smallest plant is larger in the case of
402 perpendicular movement.

403

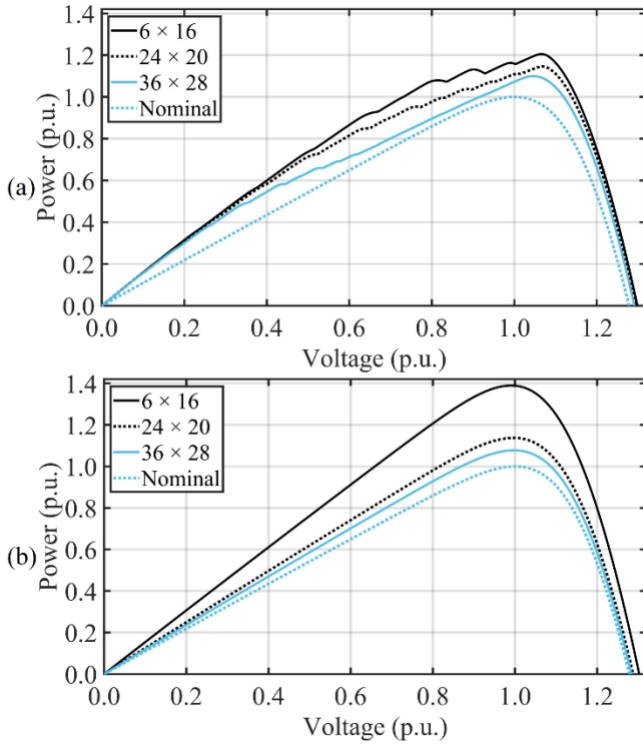


404
 405 Fig. 9. Irradiance levels received by the PV submodules of the studied PV plants at 12:34 on June 5, 2018, the time of the
 406 largest measured irradiance during the experiment. The PV plants of different sizes are presented in top of each other so
 407 that the centers coincide. The modules inside the red and blue rectangle form the 6×16 and 24×20 plant, respectively.
 408 Each row of PV modules is one string.
 409

410 Table V. Average irradiances (W/m^2) of the studied PV plants in the snapshot in Fig. 9.

PV plant	Parallel movement	Perpendicular movement
6×16	1335	1403
24×20	1286	1143
36×28	1211	1082

411
 412 The power–voltage ($P-U$) curves of the studied generators at the same time are presented in
 413 Fig. 10. In the case of parallel CE area movement, there are irradiance differences within PV module
 414 strings. These irradiance differences cause mismatch losses (Lappalainen and Valkealahti, 2017), and
 415 lead to multiple peaks in the $P-U$ curves. The global MPP powers of the generators are from 10% to
 416 20% higher than nominal due to CE. The voltages of the global MPPs are from 5% to 7% higher than
 417 the nominal. Conversely, the perpendicular movement of the CE area does not cause irradiance
 418 differences within PV strings. Thus, there are only minor mismatch losses and the $P-U$ curves are
 419 smooth (Lappalainen and Valkealahti, 2017). The global MPP powers are from 7% up to 40% larger
 420 than nominal while the global MPP voltages are close to nominal.
 421



422

423

Fig. 10. Power–voltage curves of the studied PV generators in the examples of parallel (a) and perpendicular (b) CE area movement illustrated in Fig. 9. The values are presented with respect to the nominal STC values of the generators.

424

425

426

3.4. Analysis during all the identified CE events

427

428

429

430

431

432

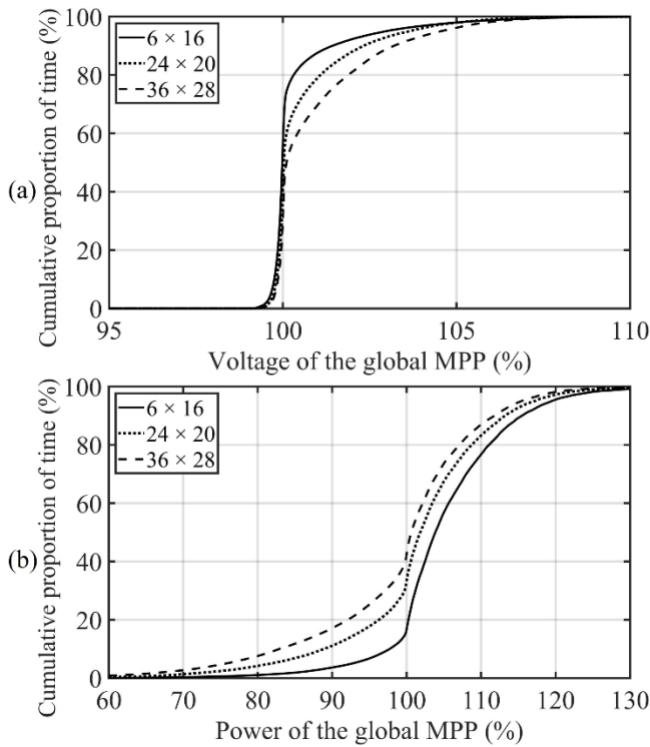
433

434

435

436

CE affects the global MPP voltages as illustrated in Fig. 10. Analysis of the operational voltage ranges of PV plants is useful to properly specify the voltage range of the inverter. Fig. 11 (a) presents the cumulative frequencies of the global MPP voltage for the studied PV generators during the identified CE events. The global MPP voltage was most of the time near the nominal value. The share of time when the global MPP voltage was higher than nominal increased with increasing generator size. The global MPP voltage was within 2% of the nominal value 87%, 79%, and 69% of the time for the 6×16 , 24×20 , and 36×28 generator, respectively. The highest global MPP voltage was about 12% higher than the nominal value for all the studied PV generators.

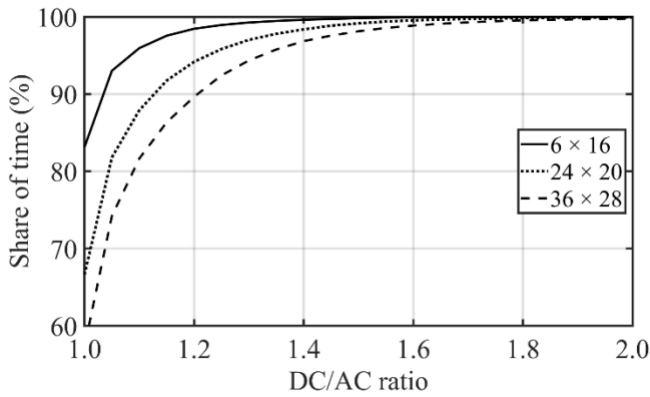


437
 438 Fig. 11. Relative cumulative frequencies of the global MPP voltage (a) and power (b) for the studied PV generators during
 439 the identified CE events. Only CE events are considered in this graph, i.e., these statistics are not representative of overall
 440 PV operation.

441
 442 The cumulative frequencies of the global MPP power are presented in Fig. 11 (b) for the
 443 studied PV generators during the identified CE events. The global MPP power during the CE events
 444 typically increased with smaller generator land area, as illustrated in Fig. 10. Thus, the share of time
 445 when the global MPP power was larger than nominal decreased with larger generator size. However,
 446 the share was over 57% for all the studied generators. The share of time when the maximum power
 447 was more than 1.2 times the nominal MPP power was from 1.8% to 4.5% depending on the generator
 448 size. The maximum instantaneous power of all the studied PV generators was over 1.4 times the
 449 nominal MPP power.

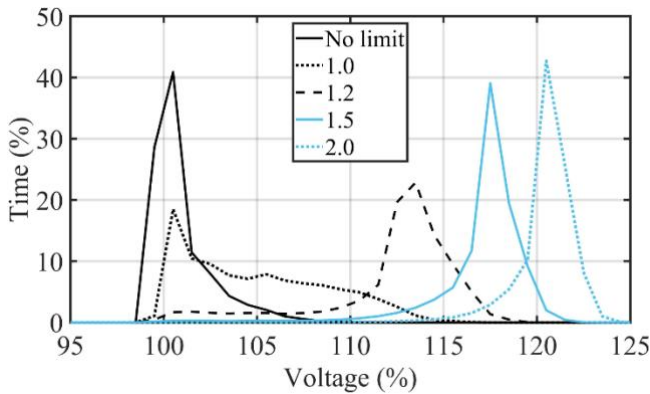
450 Fig. 12 presents the shares of time when the studied PV plants were operating in power
 451 limiting mode as a function of DC/AC ratio. The share of time when the PV plants were operating in
 452 power limiting mode increased with decreasing plant size. With a 1.0 DC/AC ratio, the PV plants
 453 were operating in power limiting mode from 57% to 83% and these shares increased rapidly with
 454 increasing DC/AC ratio. The DC/AC ratio from which the PV plant was operating more than 99% of
 455 time in power limiting mode were 1.26, 1.47, and 1.63 for the 6x16, 24x20, and 36x28 plant,
 456 respectively.

457



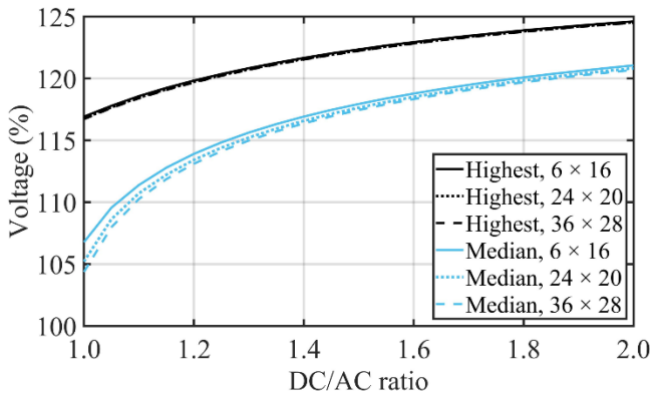
458
 459 Fig. 12. Shares of time when the studied PV plants operated in power limiting mode as a function of DC/AC ratio. Only
 460 CE events are considered in this graph, i.e., these statistics are not representative of overall PV operation.
 461

462 Fig. 13 presents the distributions of the operating voltage of the 36×28 PV plant for different
 463 DC/AC ratios. When the power of the generator was not limited, i.e., the generator operated all the
 464 time at the global MPP, the operating voltage was most of the time near the nominal MPP voltage.
 465 With a 1.0 DC/AC ratio, the peak of the voltage distribution is still near the nominal voltage, but the
 466 distribution spreads over larger voltage range. With larger DC/AC ratios, the peak of the distribution
 467 moves towards higher voltages. Moreover, the distribution becomes narrower with larger DC/AC
 468 ratio.
 469



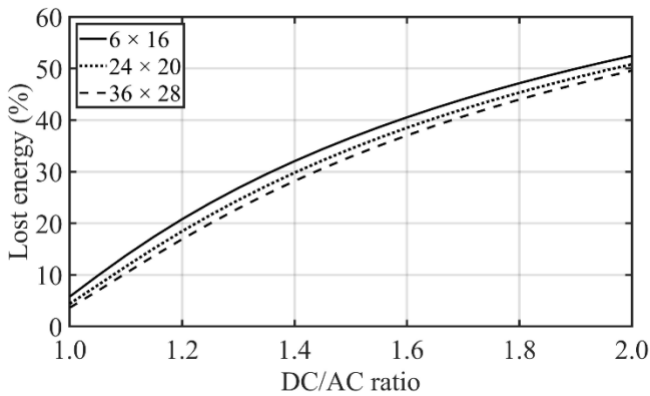
470
 471 Fig. 13. Distributions of the operating voltage of the 36×28 plant for different DC/AC ratios. The voltage is with respect
 472 to the nominal MPP voltage of the plant. Only CE events are considered in this graph, i.e., these statistics are not
 473 representative of overall PV operation.
 474

475 In Fig. 14, the highest and median operating voltages for studied PV plants are presented as a
 476 function of DC/AC ratio. There were only minor differences in the highest voltages between the
 477 studied PV plants. The highest voltages were from 17% to 25% higher than the nominal global MPP
 478 voltage. The median operating voltage increased more with increasing DC/AC ratio than the highest
 479 voltage. The operating voltage was higher for smaller plants. With DC/AC ratios larger than 1.85, the
 480 median operating voltage was over 20% higher than the nominal global MPP voltage. These results
 481 indicate that increase of operating voltage due to CE is not a major problem for PV systems.
 482



483
 484 Fig. 14. Highest and median operating voltage as a function of DC/AC ratio. The voltage is with respect to the nominal
 485 MPP voltage of the plant. Only CE events are considered in this graph, i.e., these statistics are not representative of overall
 486 PV operation.

487
 488 Operation in power limiting mode causes energy losses compared to the operation at the
 489 global MPP. These energy losses are presented in Fig. 15 for the studied PV plants as a function of
 490 DC/AC ratio. Relative energy losses due to power curtailment increased with increasing DC/AC ratio
 491 since the larger the DC/AC ratio the more the AC power is limited and the larger is the share of time
 492 spent in power limiting mode. While the differences between the studied plants were small, the
 493 relative energy losses increased with decreasing plant size. With a DC/AC ratio of 1.0, the energy
 494 losses were around 5% and with 2.0 DC/AC ratio, about half of the available energy production was
 495 lost due to power curtailment. With small DC/AC ratios, the energy losses due to power curtailment
 496 are very small given the fact that only CE events were considered.



498
 499 Fig. 15. Relative energy losses of the studied PV plants due to power curtailment as a function of DC/AC ratio. Only CE
 500 events are considered in this graph, i.e., these statistics are not representative of overall PV operation.

501
 502 **4. Discussion**

503
 504 The effects of CE on the operation of PV systems were shown to depend on the DC/AC ratio
 505 of the system. Especially, the time spent in power limiting mode and the energy losses caused by
 506 power curtailment were found to increase with increasing DC/AC ratio. With small DC/AC ratio, the
 507 increase of operating voltages as well as the energy losses due to power curtailment are small having
 508 only minor impact on the overall operation of PV systems. However, relative energy losses due to
 509 curtailment increased with increasing DC/AC ratio being around 50% for DC/AC ratio of 2.0. Thus,

510 oversizing of PV generators with respect to inverters is not recommended from the CE point of view.
511 However, PV generators are typically oversized since oversizing of the PV generators brings many
512 financial and operational benefits (Wang et al., 2018). The optimal DC/AC ratio depends on many
513 factors such as insolation conditions and inverter characteristics (Peippo and Lund, 1994). Peippo and
514 Lund (1994) stated that the optimal DC/AC ratio region is quite flat and up to 20% changes from the
515 optimal value typically leads to less than 2% losses. Zhu et al. (2011) recommended that DC/AC ratio
516 should be from 1.1 to 1.7. The results of this study show that if the intention is to avoid power
517 curtailment caused by CE, DC/AC ratio should be less than 1.0.

518 The relatively small increase of operating voltages due to CE, even with large DC/AC ratios
519 (Fig. 14) indicates that CE does not cause increased risk of short-term equipment damage or
520 disconnection for PV systems. However, the increasing operating voltage may cause further losses
521 for PV systems since the increasing DC side voltage reduces the efficiency of some inverters.
522 Moreover, the increasing operating voltage can affect the operating temperatures and lifetimes of
523 certain components used in the inverters.

524 The negative impacts of CE on the operation of PV systems decreased with increasing
525 generator size, meaning that CE is less of a problem for utility-scale PV generators. CE events that
526 have strongest impacts on the operation of PV systems are rare. In conclusion, the results of this study
527 show that CE events do not cause major problems for the operation of PV systems. However, multiple
528 assumptions and simplifications were applied in this study, which may affect the results. These issues
529 have been discussed in the following paragraphs.

530 The CE event characteristics were based on the GHI measurements by a single sensor with a
531 sampling frequency of 0.5 Hz. Measurements of multiple sensors spread over a large land area would
532 be required to measure the actual irradiances and shapes of the CE areas accurately. It has been stated
533 in Yordanov et al. (2013b) that a sampling frequency on the order of 10 Hz is needed to identify all
534 CE events. However, a sampling frequency of 0.5 Hz is high enough to identify all CE events, which
535 affect the operation of PV generators. However, the uncertainty of CE event results increases with
536 decreasing sampling frequency. Due to the low sampling frequency in our study, the durations of
537 identified CE events are underestimated, short CE events might not be identified, and several CE
538 events within a short time period might be aggregated into one event.

539 GHI measurements were used to study the effects of CE on the electrical operation of PV
540 generators. Results would be more accurate if actual plane of array irradiance measurements were
541 used. Unfortunately, those were not available. The use of actual plane of array irradiance
542 measurements would probably lead to somewhat larger CE irradiances and longer CE events.
543 However, the difference between GHI and plane of array irradiance was relatively small due to small
544 tilt angle (20°).

545 In the simulations, three assumptions were made regarding the movement of the identified CE
546 events over the PV generators (see Section 3.2). Although the assumptions are reasonable considering
547 the small sizes of the studied PV generators, the uncertainty of the results increases with larger land
548 areas. Especially, the assumption of irradiance uniformity in the cross-stream direction might not hold
549 for larger land areas. Moreover, the operating temperature of the PV generators was assumed
550 constant. The operating temperature of the PV cells of a PV generator in California, especially during
551 CE events, can be much higher than the STC temperature. The OC voltage and MPP power of a PV

552 cell decrease and the SC current increases slightly with increasing temperature. Thus, the assumption
553 of constant temperature affects mainly the results of the global MPP and operating voltages. However,
554 the use of STC temperature, which is almost always lower than real operating temperatures, leads to
555 an overestimation of the operating voltages. Thus, real operating voltages are expected to be smaller
556 than reported in this study.

557 The electrical simulation model for the PV modules naturally contains assumptions and
558 simplifications. Firstly, a PV submodule was used as a basic unit in the simulations. However, only
559 negligible irradiance differences between the PV cells of a submodule existed during the studied CE
560 events. Thus, the results of the study would change only marginally if the simulation were conducted
561 on a PV cell level. Secondly, the PV submodules were modeled by the widely used one-diode model
562 of a PV cell, which is a simplification of the more accurate two-diode model. However, the one-diode
563 model provides a good trade-off between accuracy and complexity and is accurate enough for the
564 analysis that was presented in this article. Moreover, the results could slightly change if different PV
565 modules were used as a reference for the simulation model. However, the basic behavior would not
566 change since the electrical characteristics of crystalline silicon PV modules are essentially identical.
567 Crystalline silicon was selected as it is by far the most important PV technology.

569 **5. Conclusions**

570
571 In this article, CE event characteristics and the effects of CE on the electrical operation of PV
572 generators were studied. The study was based on GHI and cloud edge velocity measurements on
573 62 days. The number, duration, and length of CE events exceeding various irradiance limits from
574 1000 W/m² over the land areas of various PV generators were studied. The average irradiance over
575 the land areas was calculated by averaging the measured GHI over a time interval defined by the ratio
576 of the PV generator dimension and the measured cloud shadow speed. Moreover, the operation of
577 three PV generators, ranging from 20 to 200 kW, was simulated during all CE events. The effects of
578 inverter sizing on the operation of the PV generators were studied by varying DC/AC ratio from 1.0
579 to 2.0.

580 In total, 2401 CE events exceeding 1000 W/m² were identified in the measured GHI. The
581 average irradiance of the 0.05 and 4 MW generator exceeded the STC irradiance over 1500 and
582 400 times, respectively. The highest measured peak irradiance was 1466 W/m² and the highest
583 average irradiances for the studied PV generator up to 1 MW generators were also over 1400 W/m².
584 The maximum durations of CE events exceeding 1300 W/m² were around one minute. The largest
585 lengths for CE events exceeding 1000 W/m² were multiple kilometers. A square-shaped PV generator
586 of up to 16 MW can occasionally be totally covered by a CE area with minimum irradiance of over
587 1200 W/m². These results mean that even large utility-scale PV power plants can be affected by CE
588 events.

589 The simulation results showed that CE affects the operation of the PV plants but the effects
590 are mainly small. Although the highest global MPP voltage and power were about 12% and 40%
591 higher than the nominal STC values, the global MPP voltage was most of the time near the nominal
592 value. The negative impacts of CE on the operation of PV systems were found to increase with
593 increasing DC/AC ratio. With a 1.0 DC/AC ratio, all the PV plants were operating in power limiting

594 mode over half of the time of the CE events and these shares increased rapidly with increasing DC/AC
595 ratio. The highest operating voltages were from 17% to 25% higher than the nominal global MPP
596 voltage. The operating voltage increased with increasing DC/AC ratio and decreasing plant size. With
597 DC/AC ratios larger than 1.85, the median operating voltage was over 20% higher than the nominal
598 global MPP voltage. The energy losses due to power curtailment were from 5% to 50% of the
599 available energy production during the CE events increasing with increasing DC/AC ratio. To avoid
600 power curtailment caused by CE, DC/AC ratios should be less than 1.0. In conclusion, the results of
601 this study show that CE do not cause major problems for the operation of PV systems.

602 **Acknowledgments**

603
604
605 The Alfred Kordelin Foundation funded the research visit of K. Lappalainen to UCSD during which
606 the study presented in this article was carried out.

607 **Data Availability Statement**

608
609
610 The data that support the findings of this study are available from the corresponding author upon
611 reasonable request.

612 **Appendix**

613
614
615 The CSS detects the component of cloud shadow velocity normal to the shadow edge, i.e.,
616 cloud shadow edge velocity, v_e (speed v_e and movement direction α_e), which underestimates the actual
617 shadow velocity v (speed v and movement direction α). A weighted non-linear regression of v and α
618 to the N_{CMV} CMVs collected in a time period of 30 min was used to calculate v from v_e as

$$619 \quad w_i v_e^i = v \cos(\alpha_e^i - \alpha), \quad (A.1)$$

620 where w_i is a weighting factor calculated as

$$621 \quad w_i = |t_f - t_0| - |t_i - t_0| + 1, \quad (A.2)$$

622 where t_f is the timestamp furthest from the present time t_0 in the time period and t_i the timestamp of
623 the i th CMV. If the CMVs collected in the time period show variation of α_e smaller than 20° , the
624 shadow movement direction is almost perpendicular to the shadow edge and the non-linear regression
625 is not needed. In these cases, and if N_{CMV} is too small for reliable regression (less than 9), the CMVs
626 are decomposed into north-south and east-west directions, and the median value of each is used to
627 recompose the resulting CMV.

628 **References**

- 629
630
631 Badescu, V., “Verification of some very simple clear and cloudy sky models to evaluate global
632 solar irradiance,” *Solar Energy* 61, 251–264 (1997).
633 Callegari, J. M. S., Cupertino, A. F., Ferreira, V. N., Brito, E. M. S., Mendes, V. F., and Pereira, H.
634 A., “Adaptive dc-link voltage control strategy to increase PV inverter lifetime,” *Microelectronics*
635 *Reliability* 100–101, 7 p. (2019).

636 Espinosa-Gavira, M. J., Agüera-Pérez, A., de la Rosa, J. J. G., Palomares-Salas, J. C., and Sierra-
637 Fernández, J. M., “An on-line low-cost irradiance monitoring network with sub-second sampling
638 adapted to small-scale PV systems,” *Sensors* 18, 12 p. (2018).

639 Gueymard, C. A., “Cloud and albedo enhancement impacts on solar irradiance using high-frequency
640 measurements from thermopile and photodiode radiometers. Part 1: Impacts on global horizontal
641 irradiance,” *Solar Energy* 153, 755–765 (2017a).

642 Gueymard, C. A., “Cloud and albedo enhancement impacts on solar irradiance using high-frequency
643 measurements from thermopile and photodiode radiometers. Part 2: Performance of separation and
644 transposition models for global tilted irradiance,” *Solar Energy* 153, 766–779 (2017b).

645 Hasegawa, K., Tsuzaki, K., and Nishizawa, S., “DC-bias-voltage dependence of degradation of
646 aluminum electrolytic capacitors,” *Microelectronics Reliability* 83, 115–118 (2018).

647 Imenes, A. G., Yordanov, G. H., Midtgård, O.-M., and Saetre, T. O., “Development of a test station
648 for accurate in situ I-V curve measurements of photovoltaic modules in Southern Norway,”
649 *Proceedings of 37th IEEE Photovoltaic Specialists Conference*, 3153–3158 (2011).

650 Järvelä, M., Lappalainen, K., and Valkealahti, S., “Cloud Enhancement Phenomenon and Its Effect
651 on PV Generators,” *Proceedings of 35th European Photovoltaic Solar Energy Conference*, 1964–
652 1968 (2018).

653 Järvelä, M., Lappalainen, K., and Valkealahti, S., “Characteristics of the cloud enhancement
654 phenomenon and PV power plants,” *Solar Energy* 196, 137–145 (2020).

655 Lappalainen, K., and Valkealahti, S., “Recognition and modelling of irradiance transitions caused by
656 moving clouds,” *Solar Energy* 112, 55–67 (2015).

657 Lappalainen, K., and Valkealahti, S., “Analysis of shading periods caused by moving clouds,” *Solar*
658 *Energy* 135, 188–196 (2016).

659 Lappalainen, K., and Valkealahti, S., “Effects of PV array layout, electrical configuration and
660 geographic orientation on mismatch losses caused by moving clouds,” *Solar Energy* 144, 548–555
661 (2017).

662 Luoma, J., Kleissl, J., and Murray, K., “Optimal inverter sizing considering cloud enhancement,”
663 *Solar Energy* 86, 421–429 (2012).

664 Mäki, A., Valkealahti, S., and Leppäaho, J., “Operation of series-connected silicon-based
665 photovoltaic modules under partial shading conditions,” *Progress in Photovoltaics: Research and*
666 *Applications* 20, 298–309 (2012).

667 do Nascimento, L. R., de Souza Viana, T., Campos, R. A., and Rüther, R., “Extreme solar
668 overirradiance events: Occurrence and impacts on utility-scale photovoltaic power plants in
669 Brazil,” *Solar Energy* 186, 370–381 (2019).

670 Ong, S., Campbell, C., Denholm, P., Margolis, R., and Heath, G., “Land-Use Requirements for Solar
671 Power Plants in the United States,”. NREL/TP-6A20-56290. Golden, CO, USA: National
672 Renewable Energy Laboratory (2013).

673 Pecenek, Z. K., Mejia, F. A., Kurtz, B., Evan, A., and Kleissl, J., “Simulating irradiance enhancement
674 dependence on cloud optical depth and solar zenith angle,” *Solar Energy* 136, 675–681 (2016).

675 Peippo, K., and Lund, P. D., “Optimal sizing of solar array and inverter in grid-connected
676 photovoltaic systems,” *Solar Energy Materials and Solar Cells* 32, 95–114 (1994).

- 677 Rampinelli, G. A., Krenzinger, A., and Chenlo Romero, F., “Mathematical models for efficiency of
678 inverters used in grid connected photovoltaic systems,” *Renewable and Sustainable Energy*
679 *Reviews* 34, 578–587 (2014).
- 680 Tapakis, R., and Charalambides, A. G., “Enhanced values of global irradiance due to the presence of
681 clouds in Eastern Mediterranean,” *Renewable Energy* 62, 459–467 (2014).
- 682 Tomson, T., “Transient processes of solar radiation,” *Theoretical and Applied Climatology* 112, 403–
683 408 (2013).
- 684 Wang, G., Kurtz, B., and Kleissl, J., “Cloud base height from sky imager and cloud speed sensor,”
685 *Solar Energy* 131, 208–21 (2016).
- 686 Wang, H. X., Munoz-García, M. A., Moreda, G. P., and Alonso-García, M. C., “Optimum inverter
687 sizing of grid-connected photovoltaic systems based on energetic and economic considerations,”
688 *Renewable Energy* 118, 709–717 (2018).
- 689 Weigl, T., Nagl, L., Weizenbeck, J., Zehner, M., Augel, M., Öchsner, P., Giesler, B., Becker, G.,
690 Mayer, O., Betts, T. R., and Gottschalg, R., “Modelling and Validation of Spatial Irradiance
691 Characteristics for Localised Irradiance Fluctuations and Enhancements,” *Proceedings of 27th*
692 *European Photovoltaic Solar Energy Conference*, 3801–3804 (2012).
- 693 Yordanov, G. H., Midtgård, O.-M., Saetre, T. O., Nielsen, H. K., and Norum, L. E., “Overirradiance
694 (Cloud Enhancement) Events at High Latitudes,” *IEEE Journal of Photovoltaics* 3, 271–277
695 (2013a).
- 696 Yordanov, G. H., Saetre, T. O., and Midtgård, O.-M., “100-millisecond Resolution for Accurate
697 Overirradiance Measurements,” *IEEE Journal of Photovoltaics* 3, 1354–1360 (2013b).
- 698 Yordanov, G. H., Saetre, T. O., and Midtgård, O.-M., “Extreme overirradiance events in Norway: 1.6
699 suns measured close to 60°N,” *Solar Energy* 115, 68–73 (2015).
- 700 Zehner, M., Weigl, T., Hartmann, M., Thaler, S., Schrank, O., Czakalla, M., Mayer, B., Betts, T. R.,
701 Gottschalg, R., Behrens, K., König-Langlo, G., Giesler, B., Becker, G., and Mayer, O., “Energy
702 Loss Due to Irradiance Enhancement,” *Proceedings of 26th European Photovoltaic Solar Energy*
703 *Conference*, 3935–3938 (2011).
- 704 Zhang, J., Watanabe, K., Yoshino, J., Kobayashi, T., Hishikawa, Y., and Doi, T., “Physical process
705 and statistical properties of solar irradiance enhancement observed under clouds,” *Japanese*
706 *Journal of Applied Physics* 57, 6 p, (2018).
- 707 Zhu, J., Bründlinger, R., Mühlberger T., Betts, T. R., and Gottschalg, R., “Optimised inverter sizing
708 for photovoltaic systems in high-latitude maritime climates,” *IET Renewable Power Generation*
709 5, 58–66 (2011).